Floquet-induced localization in long-range many-body systems

Rozhin Yousefjani [1,*] Sougato Bose,[2,†] and Abolfazl Bayat[1,‡]

[1]*Institute of Fundamental and Frontier Sciences,*
University of Electronic Science and Technology of China, Chengdu 610051, China
[2]*Department of Physics and Astronomy,*
University College London, Gower Street, London WC1E 6BT, United Kingdom

The fate of many-body localization in long-range interacting systems is not fully settled. For instance, the phase boundary between ergodic and many-body localized regimes is still under debate. Here, we use Floquet dynamics which can induce many-body localization in a clean long-range interacting system through spatio-temporal disorder, which are realized by regular operation of random local rotations. The phase diagram has been determined for two types of uniform and nonuniform long-range couplings. Our Floquet mechanism shows more localizing power than conventional static disorder methods as it pushes the phase boundary in favor of the localized phase. Moreover, our comprehensive long-time simulations provide strong support for obtained results based on static analysis.

I. INTRODUCTION

Many-Body Localization (MBL) is a profound concept in condensed matter physics for breaking the ergodicity principle [1–8]. To better understand the different aspects of MBL, several quantum information concepts [9–16] have been theoretically developed and several experiments on newly emerging quantum simulators have been performed [17–34]. Most of the MBL literature have been dedicated to 1D short-range interactions, however, several fundamental problems remain open for systems with long-range couplings [35,36]. In fact, many interactions in nature are inherently longrange, and certain quantum simulators, e.g., iontraps [17,18,37] and Rydberg atoms [19–21], are naturally governed by such interactions. Long-range couplings can exist in various forms, e.g., tunneling or Ising-type interactions, which may affect the MBL physics very differently. A key open problem in long-range MBL systems is how ergodic-MBL phase diagram changes in the presence of such long-range interactions [38–49].

Periodically driving many-body interacting systems, known as Floquet dynamics, is a well-known thermalizing mechanism [50,51], a phenomenon opposite to MBL. The fate of MBL systems under different Floquet dynamics have been studied in both theory [52–59] and experiments [32]. The results show that the MBL does not survive the Floquet dynamics unless the energy cannot be absorbed by the system due to either high frequency or large amplitude of the driving field [32,53,60,61]. Alternatively, in Refs. [62–64] the Floquet dynamics is designed to suppress the tunneling of the particles in a weakly disordered system to enhance the relative strength of disorder and interaction for generating an MBL phase. One may wonder whether it is possible to localize the evolution of a disorder-free Hamiltonian through the sequential action of local random rotations at regular time intervals. This can effectively induce spatio-temporal disorder which may localize the system. Apart from being fundamentally interesting, this has practical advantages too. In fact, inducing static disorder may result in leakage from the valid Hilbert space in superconducting quantum simulators or heating in ion-trap systems which make the simulation of the deep MBL phase very challenging [22]. Our mechanism does not suffer from this issue and thus is easier to be implemented on such quantum simulators.

In this work, we introduce a Floquet mechanism that, through generating spatio-temporal disorder, can localize a disorder-free Hamiltonian. Using this localization mechanism, we fully determine the phase diagram of two different models, namely systems with uniform and nonuniform long-range couplings. We show that our mechanism can induce MBL in certain long-range systems which cannot be localized by conventional static disordered Hamiltonians. Furthermore, through extensive long-time numerical simulations, we provide more support for our observation based on statistics of eigenstates.

The structure of the paper is as follows. After presenting the considered model in Sec. II and introducing our Floquet mechanism, the main results of the paper, namely, the phase diagram and our method for extracting the critical properties, are discussed in Sec. III. This section is followed by the dynamical analysis of the MBL phase in Sec. IV. Finally, in Sec. V, we summarize our work.

*RozhinYousefjani@uestc.edu.cn

†s.bose@ucl.ac.uk

‡abolfazl.bayat@uestc.edu.cn

II. MODEL

We consider a spin-1/2 chain of L particles interacting with long-range tunneling and Ising interaction

$$H = -\sum_{i \neq j} \left\{ \frac{J_x}{|i-j|^a} \left(S_i^x S_j^x + S_i^y S_j^y \right) + \frac{J_z}{|i-j|^b} S_i^z S_j^z \right\}. \quad (1)$$

Here $S_i^{(x,y,z)}$ is the spin-1/2 operator for qubit at site i, $J_x = J_z = 1$ are the interaction strengths, and $a, b > 0$ are the power-law exponents which determine the range of the tunneling and interaction, respectively. By varying these exponents one can tune the interaction geometry from a fully connected graph (for exponents being zero) to a local nearest-neighbor 1D chain (when the exponents tend to ∞). Many types of long-range models [35,36] such as Coulomb, van der Waals, and dipole-dipole interactions, are special cases of Hamiltonian H which can now be realized in ion trap [65,66] systems. Here, we systematically investigate two different regimes: (i) uniform couplings in which $a = b \ll \infty$; and (ii) nonuniform couplings in which b is finite (power-law Ising interaction) and $a \to \infty$ (nearest-neighbor tunneling).

To dynamically localize this disorder-free Hamiltonian, we propose a Floquet dynamic in which the evolution over a single time period τ consists of two operations. First, the system evolves under the action of the disorder-free Hamiltonian H for a short-time period τ. Second, an instant kick operation which is a set of local random rotations along the $\hat{z}$ axis, i.e., $\mathcal{R}(\boldsymbol{\theta}) = \prod_{i=1}^{L} e^{-i\theta_i S_i^z}$, rotates all the qubits without creating spin excitations, although it will induce energy excitations, in the system. Since θ_i is site-dependent, these local rotations induce spatio-temporal disorder in the dynamics of the system. The random angles $\boldsymbol{\theta} = (\theta_1, \ldots, \theta_L)$ are drawn from a uniform distribution $[-\theta/2, \theta/2]$ with $0 \leqslant \theta/\pi \leqslant 1$ being the strength of the kick. Hence, the evolution operator over a single period becomes

$$U_F(\boldsymbol{\theta}, \tau, a, b) = \mathcal{R}(\boldsymbol{\theta}) e^{-iH\tau}. \quad (2)$$

The random angles $\boldsymbol{\theta}$ remain fixed in different periods. The dynamics of the system is described by an effective Hamiltonian H_F such that $U_F = e^{-iH_F\tau}$. The random nature of $\boldsymbol{\theta}$ prevents us from analytically driving a closed form for H_F restricting us to numerical simulations. Note that, our Floquet mechanism is fundamentally different from Floquet dynamical decoupling methods [62–64] in which the suppression of the hopping amplitude increases the relative strengths of disorder and interactions that potentially drive an ergodic system toward the MBL phase.

III. PHASE DIAGRAM

Since the dynamics of the system is described by the effective Hamiltonian H_F, one can investigate the properties of this Hamiltonian to determine the phase diagram of the system as a function of parameters (θ, τ, a, b). We first investigate the statistical properties of energy levels of H_F, namely $\{E_k\}$, or equivalently the quasienergy levels of U_F given by $\{e^{-iE_k\tau}\}$. Numerically, we compute the quasi-energies using exact diagonalization of U_F in the subspace of $S_{\text{tot}}^z = 0$, with $S_{\text{tot}}^z = \sum_j S_j^z$. All the results are averaged over 1000 random samples of $\boldsymbol{\theta}$ to guarantee proper convergence. Since the Hamiltonian
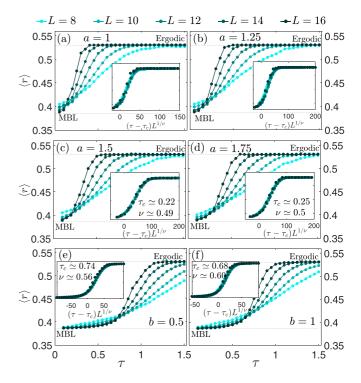

FIG. 1. Upper panels: $\langle r \rangle$ as a function of τ for uniform couplings: (a) $a = b = 1$; (b) $a = b = 1.25$; (c) $a = b = 1.5$; and (d) $a = b = 1.75$. In all panels, the results are obtained for fixed $\theta = \pi$ in systems with various sizes and the dashed lines correspond to $\langle r \rangle \simeq 0.529$ and $\langle r \rangle \simeq 0.386$ for ergodic and MBL phases, respectively. The insets are the best data collapse obtained through the finite-size scaling analysis for extracting τ_c and ν. For any choice of $a \geqslant 1.5$, our finite-size scaling analysis unambiguously determines the transition point τ_c and critical exponent ν. Since the quality of data collapse drops significantly for $a < 1.5$, despite the fact that $\langle r \rangle$ is close to 0.4 for small τ, which is possibly due to finite-size effects, no phase transition is detected for the considered system sizes. This lack of phase transition indicates that there is no localized phase for $a < 1.5$. Lower panels: $\langle r \rangle$ as a function of τ for nonuniform couplings (i.e., $b \ll a \to \infty$): (e) $b = 0.5$; and (f) $b = 1$. In both panels, we set $\theta = \pi$. The insets are the best data collapse obtained through the finite-size scaling analysis for extracting the attached transition point τ_c's and critical exponent ν's.

in Eq. (1) and its corresponding H_F are dramatically less sparse than the nearest-neighbor interactions, the numerical simulation of the system is very challenging [67] and thus is restricted to $L = 16$. By computing the consecutive energy gaps $\delta_k = E_{k+1} - E_k$, one can characterize the level statistics by their ratio $r_k = \min(\delta_{k+1}, \delta_k) / \max(\delta_{k+1}, \delta_k)$. The averaged value of this ratio, $\langle r \rangle$, serves as a well-established tool in numerical studies of finite MBL systems [68]. While the MBL phase is determined by Poisson level statistics with $\langle r \rangle \simeq 0.386$, the ergodic phase is known to follow the circular orthogonal ensemble level statistics with $\langle r \rangle \simeq 0.529$ [5,50].

Clearly, we have four control parameters in the system, namely (θ, τ, a, b). For each choice of these parameters, one can compute $\langle r \rangle$ to reveal the phase of the system. As an example, by fixing $\theta = \pi$ and considering various system sizes, in Figs. 1(a)–1(d), we plot $\langle r \rangle$ as a function of τ for several choices of uniform couplings $a = b \in \{1, 1.25, 1.5, 1.75\}$. Two

main features can be observed. First, as τ increases the system becomes ergodic and this transition gets sharper by increasing the system size. This can be understood that by increasing τ, the evolution of the disorder-free Hamiltonian H gets enough time to thermalize the system. In other words, the effective Hamiltonian H_F is dominantly determined by the Hamiltonian H rather than the disordered kick operator $\mathcal{R}(\boldsymbol{\theta})$. This is fundamentally different from those Floquet systems in which energy absorption is suppressed due to the high frequency of the ergodic evolution which makes static disorder dominant [52–59]. Second, for any choice of $a \geqslant 1.5$ [Figs. 1(c) and 1(d)] the curves of different sizes clearly intersect in tiny domains of τ, which indicates the emergence of the scale invariance in the vicinity of the transition point τ_c. Note that the intersection domains for the curves in Figs. 1(a) and 1(b), i.e., for the case $a \leqslant 1.5$, increase by adding system sizes which signal disorder-dependent transition points [45,47]. In the context of MBL, the scale invariance implies the emergence of a diverging length scale ξ in the system and thus scaling the interested observable as $\mathcal{F}(L/\xi)$. Here, $\mathcal{F}$ is an arbitrary function and L denotes the system size. Considering ergodic-MBL transition as a continuous second-order transformation results in the diverging length scale $\xi \propto |\tau - \tau_c|^{-\nu}$ with ν as the critical exponent. Precise determination of transition point τ_c and critical exponent ν demand finite-size scaling analysis. To do this, we plot $\langle r \rangle$ as a function of $(\tau - \tau_c)L^{1/\nu}$. By proper choice of τ_c and ν, one can collapse the curves for different system sizes. To achieve the best data collapse we use an elaborate optimization scheme and minimize a proper quality function Q [69–71], which is defined and discussed in the Appendix. In our case, a perfect data collapse results in $Q = 1$ and any deviation from such a perfect situation makes Q larger. Results of finite-size scaling analysis are shown in the inset of Figs. 1(a)–1(d) for uniform couplings $a = b$. While, for any choice of $a \geqslant 1.5$, the finite-size scaling unambiguously determines the transition point τ_c and critical exponent ν with $Q \sim 4$, the quality of data collapse drops significantly for $a < 1.5$. The smallest Q's for the corresponding data collapses are obtained at about 200, for any choice of τ_c and ν and considered system sizes. Therefore, for $a < 1.5$ and considered system sizes, despite the fact that $\langle r \rangle$ is close to 0.4 for small τ, which is possibly due to finite-size effects, one cannot confidently find scaling behavior which is expected near the transition point and in the thermodynamic limit, there will be no localized phase in this regime. This is an interesting observation as the power-law couplings a and b play two opposite roles. Decreasing the coupling a allows spin tunneling between the distant qubits which enhances ergodicity. On the other hand, decreasing the coupling b (i.e., making the Ising interaction more long-range) creates an effective site-dependent energy shift whose value depends on the spin configuration of the whole system. This energy shift acts like an effective random magnetic field which enhances localization. The absence of MBL in uniform couplings (i.e., $a = b$) for $a < a_c \simeq 1.5$ shows that the thermalizing long-range tunneling overcomes the localizing long-range Ising. This has also been observed in ordinary disordered long-range Hamiltonians. However, while in such systems a_c is found to be $a_c \simeq 2$ [38,41,72], our Floquet system shows more localization power with $a_c \simeq 1.5$. In other words, the spatio-
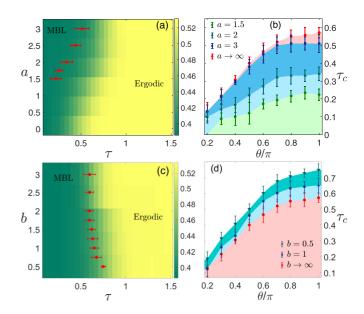

FIG. 2. Left panels: $\langle r \rangle$ for a system of length $L = 16$ and $\theta = \pi$ as a function of τ and power-law exponents for (a) uniform couplings $(a = b)$; and (c) nonuniform couplings $(b \ll a \to \infty)$. In both panels, the red markers show the MBL-ergodic phase boundary determined by the finite-size scaling analysis. Right panels: the critical τ_c as a function of θ for various choices of exponents in (b) uniform couplings $(a = b)$; and (d) nonuniform couplings $(b \ll a \to \infty)$. In both panels, the area below each curve represents the MBL phase.

temporal disorder $\mathcal{R}(\boldsymbol{\theta})$ has more localization power than the spatial one and gives $\tau_c = 0.22$ and $\tau_c = 0.25$ for $a = 1.5$ and $a = 1.75$, respectively. To investigate the phase diagram of the uniform case (i.e., $a = b$) with more details, we keep the strength of the random kick to a strong value of $\theta = \pi$ and plot $\langle r \rangle$ as a function of a and τ in Fig. 2(a) for a system of size $L = 16$. The boundary between the ergodic and the MBL phases, denoted by red markers, is determined by finite-size scaling analysis of $\langle r \rangle$, as discussed before. In addition, to clarify the role of random kick strength, in Fig. 2(b) we plot the critical time τ_c as a function of θ for various a's. The area below each curve represents the MBL phase. Clearly, by reducing a the MBL area shrinks, showing the tendency toward thermalization.

All the above analysis can be repeated for systems with nonuniform couplings $(b \ll a \to \infty)$. Again as an example, by fixing $\theta = \pi$ and considering various system sizes, in Figs. 1(e) and 1(f), we plot $\langle r \rangle$ as a function of τ for two choices of nonuniform couplings $b \in \{0.5, 1\}$. For considered system sizes, one can see the clear intersection points for all the curves in Figs. 1(e) and 1(f) which determine the onset of transition. The finite-size scaling analysis which collapses all the curves on a universal one as a function of $(\tau - \tau_c)L^{1/\nu}$ and leads to precise τ_c are presented in the insets of Figs. 1(e) and 1(f). The achieved Q's for these data collapses are about four. As long-range Ising interaction induces an effective static disorder in the chain, the free evolution of the clean Hamiltonian H takes a longer time to thermalize the system. Therefore the transition points are highly skewed to the larger values of τ. We obtain $\tau_c = 0.74$ and $\tau_c = 0.68$ for systems with nonuniform couplings $b = 0.5$ and $b = 1$, respectively.
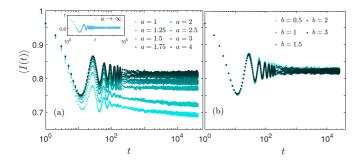
FIG. 3. Imbalance $\langle I(t) \rangle$ versus t in the MBL phase for $\theta = \pi$, $\tau = 0.1$, and $L = 16$. Panel (a) and its inset are for the uniform couplings ($a = b$). Panel (b) is for the nonuniform couplings ($b \ll a \to \infty$).

To determine the whole phase diagram of the system for nonuniform couplings, in Fig. 2(c), we plot $\langle r \rangle$ as a function of b and τ in a system of size $L = 16$, when the strength of the disordered kick is fixed to $\theta = \pi$. The phase boundary between the MBL and the ergodic phases in Fig. 2(b) are denoted by red markers. By decreasing b (i.e., making the Ising interaction more longrange) the localization power enhances and the system can localize for longer τ. As discussed above, decreasing b induces effective disorder and thus τ_c is increased. To see the effect of disordered kick strength on the phase diagram, in Fig. 2(d) we plot τ_c as a function of θ for various b's. The area below the curves represents the MBL phase. As expected, by decreasing b the MBL region increases which further confirms the enhancement of the localization power.

IV. DYNAMICAL ANALYSIS OF THE MBL PHASE

To better understand the MBL phase in long-range interacting systems, it is highly insightful to investigate the dynamical properties. Here, we focus on measuring imbalance that can quantify the ability of the system to conserve the initial information. In fact, we pursue two main objectives: (i) illustrating the localization dynamics of the system; and (ii) providing further affirmation for the phase boundary determined by $\langle r \rangle$, in particular the absence of MBL for $a = b < 1.5$.

We initialize a system of size $L = 16$ in Néel state $|\psi(0)\rangle = |\uparrow\downarrow\ldots\uparrow\downarrow\rangle$. The evolution of the system after t times kicking is given by $|\psi(t)\rangle = (U_F)^t|\psi(0)\rangle$. The imbalance is defined as $I(t) = 2/L \sum_i (-1)^{i+1} \langle S_i^z \rangle$, where $\langle S_i^z \rangle = \langle \psi(t)|S_i^z|\psi(t)\rangle$ and the normalization in the definition guarantees that $I(0) = 1$. In the following, we set $\theta = \pi$ and $\tau = 0.1$ to be sure that the system evolves in MBL phase. For achieving good statistics and converging results, we generate 1000 random samples and denote the random-averaged imbalance as $\langle I(t) \rangle$. While in the ergodic phase, the imbalance has to relax to zero, showing no memory about the initial state, in the MBL phase it reaches a finite value, resembling the presence of memory [12,29,32]. Figure 3(a) illustrates random-averaged imbalance $\langle I(t) \rangle$ versus t for various values of uniform couplings ($a = b$). After a transport time, the imbalance relaxes to a plateau for $a \geqslant 1.5$, signaling that the system is strongly localized and all particles will stay close to their original positions during time evolution. This is in full agreement with the level statistics analysis presented in the

previous section. For $a < 1.5$ the imbalance gradually relaxes to zero and, hence, the system will thermalize in a longtime. This confirms that for the choice of $\tau = 0.1$, $\theta = \pi$ the critical power-law coupling is $a_c \simeq 1.5$, again in agreement with level statistics analysis. For the sake of completeness, in the inset of Fig. 3(a) we plot the random-averaged imbalance for a system with short-range tunneling and Ising interaction, i.e., $a = b \to \infty$. For nonuniform couplings, in Fig. 3(b), we plot the imbalance as a function of t for various b's. Interestingly, in the localized phase the dynamics of imbalance and its saturation hardly changes by b. Clearly, all the curves after some transport time relax to a nonzero constant showing that system can preserve the initial information during the long-time simulation.

V. CONCLUSION

We have proposed a Floquet mechanism, which enables the creation of the MBL phase in a disorder-free long-range interacting system. In the limit of short-time evolution τ, the mechanism reproduces the results for conventional disordered systems. By utilizing this Floquet mechanism, two main results have been achieved. Firstly, we have determined the phase diagram of the system for two different types of couplings, namely uniform ($a = b$) and nonuniform ($b \ll a \to \infty$), using level statistics. Our mechanism shows a strong localizing power such that it prevents thermalization in those long-range systems which cannot be localized merely by disorder. Second, we have studied the dynamics of imbalance to provide further support for the level-statistics analysis in both types of couplings.

APPENDIX

To precisely determine the critical values, we perform finite-size scaling analysis using Python package pyfssa and evaluate the quality of the data collapse as follows. Assuming that i indexes the system size L_i and j indexes the time period τ_j with $\tau_1 < \tau_2 < \cdots < \tau_k$. For scaled observations $\{y_{ij}\}$ (e.g., the random-averaged level statistics ratio $\langle r \rangle$) and its standard errors $\{dy_{ij}\}$ at $x_{ij} = L_i^{1/\nu}(\tau_j - \tau_c)$, and also $\{\hat{y}_{ij}\}$ and $\{d\hat{y}_{ij}\}$ as the estimated values of the master curve and its standard error again at $x_{ij} = L_i^{1/\nu}(\tau_j - \tau_c)$, Houdayer and Hartmann [71] redefined the quality function

$$Q = \frac{1}{N} \sum_{ij} \frac{(y_{ij} - \hat{y}_{ij})^2}{dy_{ij}^2 - d\hat{y}_{ij}^2}. \quad \text{(A1)}$$

The sum in the quality function Q only involves terms for which the estimated value $\hat{y}_{ij}$ of the master curve at x_{ij} is defined. The number of such terms is $\mathcal{N}$. For an optimal fit,

the individual deviations $(y_{ij} - \hat{y}_{ij})^2$ is of the order of the individual error $dy_{ij}^2 - d\hat{y}_{ij}^2$, so the quality Q is close to one and much larger for nonoptimal fits.

[1] E. Altman, Many-body localization and quantum thermalization, Nat. Phys. **14**, 979 (2018).

[2] D. A. Abanin and Z. Papi, Recent progress in many-body localization, Annalen der Physik **529**, 1700169 (2017).

[3] M. Serbyn, Z. Papić, and D. A. Abanin, Local Conservation Laws and the Structure of the Many-Body Localized States, Phys. Rev. Lett. **111**, 127201 (2013).

[4] D. A. Abanin, E. Altman, I. Bloch, and M. Serbyn, Colloquium: Many-body localization, thermalization, and entanglement, Rev. Mod. Phys. **91**, 021001(2019).

[5] D. J. Luitz, N. Laflorencie, and F. Alet, Many-body localization edge in the random-field Heisenberg chain, Phys. Rev. B **91**, 081103(R) (2015).

[6] V. Khemani, S. P. Lim, D. N. Sheng, and D. A. Huse, Critical Properties of the Many-Body Localization Transition, Phys. Rev. X **7**, 021013 (2017).

[7] A. Pal and D. A. Huse, Many-body localization phase transition, Phys. Rev. B **82**, 174411 (2010).

[8] S. Iyer, V. Oganesyan, G. Refael, and D. A. Huse, Many-body localization in a quasiperiodic system, Phys. Rev. B **87**, 134202 (2013).

[9] J. Gray, S. Bose, and A. Bayat, Many-body localization transition: Schmidt gap, entanglement length, and scaling, Phys. Rev. B **97**, 201105(R) (2018).

[10] J. Gray, A. Bayat, A. Pal, and S. Bose, Scale Invariant Entanglement Negativity at the Many-Body Localization Transition, arXiv:1908.02761.

[11] A. Nico-Katz, A. Bayat, and S. Bose, Information-theoretic memory scaling in the many-body localization transition, Phys. Rev. B **105**, 205133 (2022).

[12] A. Nico-Katz, A. Bayat, and S. Bose, A Memory Hierarchy for Many-Body Localization: Emulating the Thermodynamic Limit, arXiv:2111.01146.

[13] G. De Tomasi, S. Bera, J. H. Bardarson, and F. Pollmann, Quantum Mutual Information as a Probe for Many-Body Localization, Phys. Rev. Lett. **118**, 016804 (2017).

[14] Z.-H. Sun, J. Cui, and H. Fan, Characterizing the many-body localization transition by the dynamics of diagonal entropy, Phys. Rev. Res. **2**, 013163 (2020).

[15] M. Kiefer-Emmanouilidis, R. Unanyan, M. Fleischhauer, and J. Sirker, Evidence for Unbounded Growth of the Number Entropy in Many-Body Localized Phases, Phys. Rev. Lett. **124**, 243601 (2020).

[16] R. Ghosh and M. Žnidarič, Resonance-induced growth of number entropy in strongly disordered systems, Phys. Rev. B **105**, 144203 (2022).

[17] J. Smith, A. Lee, P. Richerme, B. Neyenhuis, P. W. Hess, P. Hauke, M. Heyl, D. A. Huse, and C. Monroe, Many-body localization in a quantum simulator with programmable random disorder, Nat. Phys. **12**, 907 (2016).

[18] W. Morong, F. Liu, P. Becker, K. S. Collins, L. Feng, A. Kyprianidis, G. Pagano, T. You, A. V. Gorshkov, and C. Monroe, Observation of stark many-body localization without disorder, Nature (London) **599**, 393 (2021).

[19] J.-y. Choi, S. Hild, J. Zeiher, P. Schau, A. Rubio-Abadal, T. Yefsah, V. Khemani, D. A. Huse, I. Bloch, and C. Gross, Exploring the many-body localization transition in two dimensions, Science **352**, 1547 (2016).

[20] M. Rispoli, A. Lukin, R. Schittko, S. Kim, M. E. Tai, J. Léonard, and M. Greiner, Quantum critical behaviour at the many-body localization transition, Nature (London) **573**, 385 (2019).

[21] A. Lukin, M. Rispoli, R. Schittko, M. E. Tai, A. M. Kaufman, S. Choi, V. Khemani, J. Léonard, and M. Greiner, Probing entanglement in a many-body-localized system, Science **364**, 256 (2019).

[22] M. Gong, G. D. de Moraes Neto, C. Zha, Y. Wu, H. Rong, Y. Ye, S. Li, Q. Zhu, S. Wang, Y. Zhao, F. Liang, J. Lin, Y. Xu, C.-Z. Peng, H. Deng, A. Bayat, X. Zhu, and J.-W. Pan, Experimental characterization of the quantum many-body localization transition, Phys. Rev. Res. **3**, 033043 (2021).

[23] Q. Guo, C. Cheng, Z.-H. Sun, Z. Song, H. Li, Z. Wang, W. Ren, H. Dong, D. Zheng, Y.-R. Zhang, R. Mondaini, H. Fan, and H. Wang, Observation of energy-resolved many-body localization, Nat. Phys. **17**, 234 (2021).

[24] C. Zha, V. M. Bastidas, M. Gong, Y. Wu, H. Rong, R. Yang, Y. Ye, S. Li, Q. Zhu, S. Wang, Y. Zhao, F. Liang, J. Lin, Y. Xu, C. Z. Peng, J. Schmiedmayer, K. Nemoto, H. Deng, W. J. Munro, X. Zhu *et al.*, Ergodic-Localized Junctions in a Periodically Driven Spin Chain, Phys. Rev. Lett. **125**, 170503 (2020).

[25] K. Xu, J.-J. Chen, Y. Zeng, Y.-R. Zhang, C. Song, W. Liu, Q. Guo, P. Zhang, D. Xu, H. Deng *et al.*, Emulating Many-Body Localization with a Superconducting Quantum Processor, Phys. Rev. Lett. **120**, 050507 (2018).

[26] B. Chiaro, C. Neill, A. Bohrdt, M. Filippone, F. Arute, K. Arya, R. Babbush, D. Bacon, J. Bardin, R. Barends, S. Boixo, D. Buell, B. Burkett, Y. Chen, Z. Chen, R. Collins, A. Dunsworth, E. Farhi, A. Fowler, B. Foxen *et al.*, Direct measurement of non-local interactions in the many-body localized phase, arXiv:1910.06024.

[27] Q. Guo, C. Cheng, H. Li, S. Xu, P. Zhang, Z. Wang, C. Song, W. Liu, W. Ren, H. Dong *et al.*, Stark Many-Body Localization on a Superconducting Quantum Processor, Phys. Rev. Lett. **127**, 240502 (2021)

[28] X. Mi, M. Ippoliti, C. Quintana, A. Greene, Z. Chen, J. Gross, F. Arute, K. Arya, J. Atalaya, R. Babbush, J. C. Bardin, J. Basso, A. Bengtsson, A. Bilmes, A. Bourassa, L. Brill, M. Broughton, B. B. Buckley, D. A. Buell, B. Burkett *et al.*, Time-crystalline eigenstate order on a quantum processor, Nature (London) **601**, 531 (2022).

[29] M. Schreiber, S. S. Hodgman, P. Bordia, H. P. Lüschen, M. H. Fischer, R. Vosk, E. Altman, U. Schneider, and I. Bloch, Observation of many-body localization of interacting fermions in a quasirandom optical lattice, Science **349**, 842 (2015).

[30] S. S. Kondov, W. R. McGehee, W. Xu, and B. DeMarco, Disorder-Induced Localization in a Strongly Correlated Atomic Hubbard Gas, Phys. Rev. Lett. **114**, 083002 (2015).

[31] P. Bordia, H. Lüschen, S. Scherg, S. Gopalakrishnan, M. Knap, U. Schneider, and I. Bloch, Probing Slow Relaxation and Many-Body Localization in Two-Dimensional Quasiperiodic Systems, Phys. Rev. X **7**, 041047 (2017).

[32] P. Bordia, H. Lüschen, U. Schneider, M. Knap, and I. Bloch, Periodically driving a many-body localized quantum system, Nat. Phys. **13**, 460 (2017).

[33] S. Choi, J. Choi, R. Landig, G. Kucsko, H. Zhou, J. Isoya, F. Jelezko, S. Onoda, H. Sumiya, V. Khemani, C. von Keyserlingk, N. Y. Yao, E. Demler, and M. D. Lukin, Observation of discrete time-crystalline order in a disordered dipolar many-body system, Nature (London) **543**, 221 (2017).

[34] J. Choi, H. Zhou, S. Choi, R. Landig, W. W. Ho, J. Isoya, F. Jelezko, S. Onoda, H. Sumiya, D. A. Abanin, and M. D. Lukin, Probing Quantum Thermalization of a Disordered Dipolar Spin Ensemble with Discrete Time-Crystalline Order, Phys. Rev. Lett. **122**, 043603 (2019).

[35] N. Defenu, T. Donner, T. Macr, G. Pagano, S. Ruffo, and A. Trombettoni, Long-range interacting quantum systems, arXiv:2109.01063.

[36] D. Lewis, A. Benhemou, N. Feinstein, L. Banchi, and S. Bose, Optimal Quantum Spatial Search with One-Dimensional Long-Range Interactions, Phys. Rev. Lett. **126**, 240502 (2021).

[37] F. Rajabi, S. Motlakunta, C.-Y. Shih, N. Kotibhaskar, Q. Quraishi, A. Ajoy, and R. Islam, Dynamical Hamiltonian engineering of 2D rectangular lattices in a one-dimensional ion chain, npj Quantum Inf. **5**, 32 (2019).

[38] X. Deng, G. Masella, G. Pupillo, and L. Santos, Universal Algebraic Growth of Entanglement Entropy in Many-Body Localized Systems with Power-Law Interactions, Phys. Rev. Lett. **125**, 010401 (2020).

[39] S. Roy and D. E. Logan, Self-consistent theory of many-body localisation in a quantum spin chain with long-range interactions, SciPost Phys. **7**, 042 (2019).

[40] R. M. Nandkishore and S. L. Sondhi, Many-Body Localization with Long-Range Interactions, Phys. Rev. X **7**, 041021 (2017).

[41] N. Y. Yao, C. R. Laumann, S. Gopalakrishnan, M. Knap, M. Müller, E. A. Demler, and M. D. Lukin, Many-Body Localization in Dipolar Systems, Phys. Rev. Lett. **113**, 243002 (2014).

[42] R. Modak and T. Nag, Many-body localization in a long-range model: Real-space renormalization-group study, Phys. Rev. E **101**, 052108 (2020).

[43] A. L. Burin, Localization in a random xy model with long-range interactions: Intermediate case between single-particle and many-body problems, Phys. Rev. B **92**, 104428 (2015).

[44] S. Schiffer, J. Wang, X.-J. Liu, and H. Hu, Many-body localization in *xy* spin chains with long-range interactions: An exact-diagonalization study, Phys. Rev. A **100**, 063619 (2019).

[45] A. L. Burin, Many-body delocalization in a strongly disordered system with long-range interactions: Finite-size scaling, Phys. Rev. B **91**, 094202 (2015).

[46] K. S. Tikhonov and A. D. Mirlin, Many-body localization transition with power-law interactions: Statistics of eigenstates, Phys. Rev. B **97**, 214205 (2018).

[47] A. O. Maksymov and A. L. Burin, Many-body localization in spin chains with long-range transverse interactions: Scaling of critical disorder with system size, Phys. Rev. B **101**, 024201 (2020).

[48] H. Li, J. Wang, X.-J. Liu, and H. Hu, Many-body localization in ising models with random long-range interactions, Phys. Rev. A **94**, 063625 (2016).

[49] S. J. Thomson and M. Schiró, Quasi-many-body localization of interacting fermions with long-range couplings, Phys. Rev. Res. **2**, 043368 (2020).

[50] L. D'Alessio and M. Rigol, Long-time Behavior of Isolated Periodically Driven Interacting Lattice Systems, Phys. Rev. X **4**, 041048 (2014).

[51] A. Lazarides, A. Das, and R. Moessner, Equilibrium states of generic quantum systems subject to periodic driving, Phys. Rev. E **90**, 012110 (2014).

[52] P. Ponte, A. Chandran, Z. Papi, and D. A. Abanin, Periodically driven ergodic and many-body localized quantum systems, Ann. Phys. **353**, 196 (2015).

[53] A. Lazarides, A. Das, and R. Moessner, Fate of Many-Body Localization Under Periodic Driving, Phys. Rev. Lett. **115**, 030402 (2015).

[54] H. Burau, M. Heyl, and G. De Tomasi, Fate of algebraic many-body localization under driving, Phys. Rev. B **104**, 224201 (2021).

[55] L. Zhang, V. Khemani, and D. A. Huse, A floquet model for the many-body localization transition, Phys. Rev. B **94**, 224202 (2016).

[56] D. S. Bhakuni and A. Sharma, Stability of electric field driven many-body localization in an interacting long-range hopping model, Phys. Rev. B **102**, 085133 (2020).

[57] M. Sarkar, R. Ghosh, A. Sen, and K. Sengupta, Signatures of multifractality in a periodically driven interacting Aubry-André model, Phys. Rev. B **105**, 024301 (2022).

[58] M. Mierzejewski, K. Giergiel, and K. Sacha, Many-body localization caused by temporal disorder, Phys. Rev. B **96**, 140201(R) (2017).

[59] P. Ponte, Z. Papić, F. m. c. Huveneers, and D. A. Abanin, Many-Body Localization in Periodically Driven Systems, Phys. Rev. Lett. **114**, 140401 (2015).

[60] A. Haldar, R. Moessner, and A. Das, Onset of floquet thermalization, Phys. Rev. B **97**, 245122 (2018).

[61] A. Haldar, D. Sen, R. Moessner, and A. Das, Dynamical Freezing and Scar Points in Strongly Driven Floquet Matter: Resonance vs Emergent Conservation Laws, Phys. Rev. X **11**, 021008 (2021).

[62] E. Bairey, G. Refael, and N. H. Lindner, Driving induced many-body localization, Phys. Rev. B **96**, 020201 (2017).

[63] S. Choi, D. A. Abanin, and M. D. Lukin, Dynamically induced many-body localization, Phys. Rev. B **97**, 100301 (2018).

[64] D. S. Bhakuni, R. Nehra, and A. Sharma, Drive-induced many-body localization and coherent destruction of stark many-body localization, Phys. Rev. B **102**, 024201 (2020).

[65] P. Jurcevic, B. P. Lanyon, P. Hauke, C. Hempel, P. Zoller, R. Blatt, and C. F. Roos, Quasiparticle engineering and entanglement propagation in a quantum many-body system, Nature (London) **511**, 202 (2014).

[66] P. Richerme, Z.-X. Gong, A. Lee, C. Senko, J. Smith, M. Foss-Feig, S. Michalakis, A. V. Gorshkov, and C. Monroe, Non-local propagation of correlations in quantum systems with long-range interactions, Nature (London) **511**, 198 (2014).

[67] P. Secular, N. Gourianov, M. Lubasch, S. Dolgov, S. R. Clark, and D. Jaksch, Parallel time-dependent variational principle algorithm for matrix product states, Phys. Rev. B **101**, 235123 (2020).

[68] V. Oganesyan and D. A. Huse, Localization of interacting fermions at high temperature, Phys. Rev. B **75**, 155111 (2007).

[69] A. Sorge, pyfssa 0.7.6. Zenodo. (2015), https://zenodo.org/badge/latestdoi/6089/andsor/pyfssa.

[70] O. Melchert, autoScale.py - A program for automatic finite-size scaling analyses: A user's guide, arXiv:0910.5403.

[71] J. Houdayer and A. K. Hartmann, Low-temperature behavior of two-dimensional gaussian ising spin glasses, Phys. Rev. B **70**, 014418 (2004).

[72] A. Safavi-Naini, M. L. Wall, O. L. Acevedo, A. M. Rey, and R. M. Nandkishore, Quantum dynamics of disordered spin chains with power-law interactions, Phys. Rev. A **99**, 033610 (2019).